Research Article | Vol. 9, No. 10 / 1 October 2019 / Optical Materials Express 4070
Optical Materials EXPRESS

See-through reflective metasurface diffraction grating

DANIEL K. NIKOLOV,[1] FEI CHENG,[1] LEI DING,[1] AARON BAUER,[1] A. NICK VAMIVAKAS,[1,2,3,4] AND JANNICK P. ROLLAND[1,4,5,*]

[1] Institute of Optics, University of Rochester, 480 Intercampus Dr, Rochester, NY 14627, USA
[2] Department of Physics, University of Rochester, 500 Wilson Blvd, Rochester, NY 14627, USA
[3] Center for Coherence and Quantum Optics, University of Rochester, Rochester, NY 14627, USA
[4] Materials Science, University of Rochester, Rochester, NY 14627, USA
[5] Center for Freeform Optics, University of Rochester, Rochester, NY 14627, USA
[*] rolland@optics.rochester.edu

Abstract: Metal-dielectric reflective metasurfaces with an engineered phase response provide a versatile alternative to conventional optics, especially when wanting to defy the basic law of reflection, as in compact near-eye display systems for augmented reality applications. Specifically, a key component of these display systems is a reflective grating with see-through function or capability. For a reflective metasurface, the transmission regime is typically not allowed due to a non-transparent metal backplate. In the current work, we propose a method to enable see-through metal-dielectric metasurfaces by etching apertures of random position and diameter (RPD) much larger than the design wavelength of the metasurfaces. We demonstrate a 1200 lp/mm metal-dielectric metasurface diffraction grating for use in reflection with 650 nm illumination. The fabricated device shows ~20% diffraction efficiency in the first diffractive order over 0-50° angle of incidence, which is in agreement with the electromagnetic simulations. The device is semitransparent, letting ~50% of the light illuminating the back of the device through via the RPD apertures. Furthermore, the light transmitted through the RPD apertures does not show any defined features due to diffraction (rings, fringes, etc.) aside from a quasi-uniform halo.

1. Introduction

Diffractive gratings have a variety of applications in emerging optical domains such as the design of head-worn displays (HWDs) [1–4]. Gratings used in HWDs must be robust enough for a consumer device, operate in reflection in the visible regime to relay a virtual image to the eye as a part of a waveguide relay [5–9] or serve as a reflective combiner [10,11]. In the later function, it must also be see-through in transmission, so the combiner does not obscure the real world [see Fig. 1(a)].

Recently it has been shown that metasurface devices can be used to replace traditional optical elements such as lenses [12], polarizers [13,14] and holograms [15]. In particular, successful implementation of reflective diffraction gratings using metal-dielectric-metal metasurfaces has been demonstrated in the infrared [16,17] and the visible [18,19]. Organic polymers such as polymethyl methacrylate (PMMA) have been used to increase the robustness of these structures for consumer devices use by preventing metal degradation [20–24].

A key component of reflective metasurface devices is an opaque metal backplate (with the thickness on the scale of tens to hundreds of nm) that allows the phase of the reflected wavefront to be tuned between $-\pi$ and π. This non-transparent plate cannot be used in an HWD waveguide relay or combiner as it will obscure the user's view of the real world. It should be noted that previous work has shown that noble metal films can be semi-transparent for visible light illuminating films with critical thickness (2-6 nm for Ag films in particular) [25]. In this regime

#367749 https://doi.org/10.1364/OME.9.004070
Journal © 2019 Received 20 May 2019; revised 22 Aug 2019; accepted 3 Sep 2019; published 16 Sep 2019

Optical Materials EXPRESS

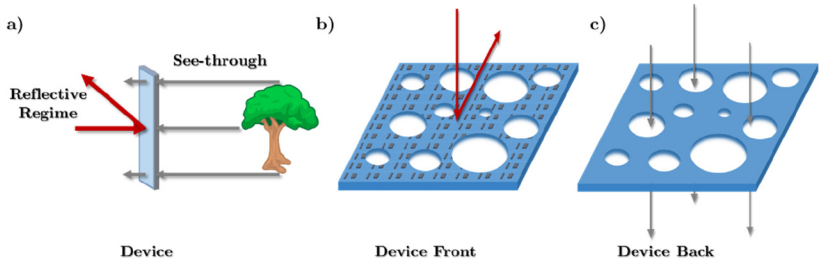

Fig. 1. The device application. (a) There are two working regimes – reflective and see-through. The reflective side provides arbitrary optical function. Light illuminating the device from the back side gets transmitted through with minimal alterations. (b) The reflective side of the device. The rectangular nano-tokens shape the reflected wavefront. (c) The back side of the device. The large circular apertures provide the see-through property. The device was rotated to match the orientation in (b) for easier comparison.

the metal transitions from continuous to islands film. The anomalous transmission is due to localized plasmons whose intensity and frequency are determined by the dimensions of the islands [26–27]. The modeling of this ultrathin, quasi-continuous film deposition and the effect of these localized plasmons on the anomalous reflection of metal-dielectric-metal metasurface devices (assuming the use of metal films with critical thickness as a backplate) together with the fabrication of these films is quite challenging.

Here, we propose an alternative way to achieve semi-transparency while preserving the anomalous reflection illustrated in Fig. 2. Specifically, we propose etching a set of circular apertures with diameters much larger than the wavelength of operation. The advantage of this method is that a see-through function of the device can be achieved with a continuous metal backplate with thickness (tens to hundreds of nm) much higher than the critical thickness. These apertures are large enough (i.e. tens of microns) that they will not interfere with the grating function in reflection, while also being small enough that they will be invisible to the human eye. Furthermore, by increasing the total area covered by the apertures as desired, an arbitrary high see-through ratio can be achieved for all visible light. However, such an array of apertures can generate various undesirable diffraction artifacts in the transmitted light [28–30].

In the current work, we design and demonstrate a metal-dielectric metasurface device that behaves as a grating in reflection and is see-through in transmission. An array of apertures of random position and diameter (RPD) is created on the device to provide a desired transmission ratio while avoiding the undesirable diffraction artifacts.

Optical Materials EXPRESS

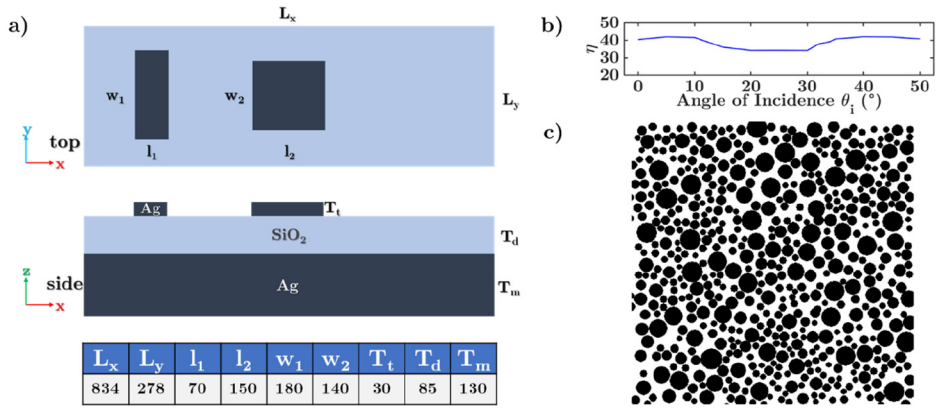

L_x	L_y	l_1	l_2	w_1	w_2	T_t	T_d	T_m
834	278	70	150	180	140	30	85	130

Fig. 2. (a) The unit cell for the final designed metasurface – top x-y and side x-z view (diagram) including dimensions in nm (table); (b) the modeled efficiency of the first diffractive order for AOIs from 0 to 50°. (c) The random position and diameter of the pattern of apertures that is superimposed on the metasurface design shown in (a) to enable the see-through regime. The aperture sizes vary between 8 um and 30 μm.

2. Simulations and modeling

For the current work, our goal is to design and fabricate a device that functions as a 1200 lp/mm diffractive grating in reflection with a 650 nm illumination wavelength and transmits 50% of all visible light that illuminates the device from the back. The diffraction efficiency in the first diffractive order in reflection is ~20% and needs to be uniform for angles of incidence (AOI) θ_i ranging from 0 to 50 degrees. An example of back illumination in a consumer device may be the bright white light of approaching vehicles while driving. The see-through regime combined with the flat diffractive efficiency in reflection will allow such device to be used in a variety of optical systems with wide field-of-view (FOV) including but not limited to HWDs.

To achieve a $-\pi$ to π linear phase response in reflection, we pattern the front of the device with Ag nano-tokens of varying dimensions like in our previous work on metal-dielectric-metal gratings [24]. Unit cells of dimensions $L_x = 834$ nm by $L_y = 278$ nm are chosen to meet the 1200 lp/mm specification for the grating as shown in Fig. 2(a). SiO_2 is used for the dielectric insulator and Ag is chosen for the metal backplate. The thicknesses of each layer are listed in the table in Fig. 2(a).

The unit cell is further split in three square regions of 278 × 278 nm^2. A commercial finite-difference-time-domain software [31] was used to perform a parameter sweep calculating the individual amplitude and phase response of tokens with varying x and y dimensions and normal AOI illumination. A token with specific width and height is chosen for each square to approximate the linear grating response as a step-wise function based on the parameter sweep results [19]. During the design process, we established that the third token had the smallest dimension and could be removed without significantly affecting the overall efficiency and phase gradient of the grating. This decreased complexity of the design allows for an easier fabrication process. The dimensions of the final set of tokens are listed in Fig. 2(a). The full unit cell was modeled using anti-symmetric boundary conditions along the y-axis, Bloch boundary conditions along the x-axis, and a perfectly matched layer (PML) boundary conditions along the z-axis. A parameter sweep varying the AOI of the incoming illumination was completed evaluating the diffraction efficiency of the first diffractive order using a frequency-domain field monitor for each AOI. The resulting nominal efficiency as a function of AOI is presented in Fig. 2(b). It should be noted that the optimized efficiency over a broad range of AOIs is 40% for the grating shown

Optical Materials EXPRESS

in Fig. 2(a), which is twice that of the of the final device accounting for the 50% see-through transmission.

To create the RPD aperture pattern we developed a MATLAB script that generates the fabrication files used in the optical lithography process. Initial modeling and testing showed that using apertures of a fixed size or position creates unwanted diffraction artifacts of the transmitted light. These artifacts included lines, colored rings and other artifacts with well-defined structure. We eliminated these artifacts by randomizing the position and diameter of the apertures. We discuss the resulting performance in more details in the following section.

First, we consider the numerical generation of the RPD aperture patterns. The optical lithography files required to etch the apertures take as input the position and diameter of the circular apertures. It is required for the apertures to not overlap and for the fraction of the overall area covered by the RPD aperture pattern to be equal to the target transmission ratio specification (50% in the current work). The complete RPD aperture pattern is generated iteratively. A random position within the sample dimensions (834 μm by 834 μm) is chosen followed by a random radius varying between 8 μm and 30 μm. This range of aperture radii was chosen such that the apertures are large enough to be easily pattern transferred using optical lithography and etching while also being small enough not to be seen by the naked eye. If the aperture is fully within the sample, its area, position and radius are recorded. A second aperture is then selected. If it intersects with the first aperture, it is dropped, and another random aperture is generated. If it does not intersect with any existing aperture, its area, position and radius are stored. This process is repeated until the sum of the area of all stored apertures covers the area matching the required transmission ratio.

The described procedure can be computationally heavy for large samples. To avoid unreasonably long file generation times, we segment the full sample in smaller regions and generate the RPD aperture pattern for each region individually to satisfy the required transmission ratio. To avoid having continuous streaks between regions that can cause diffraction artifacts we allow the apertures from each region to overflow into the neighboring region. The pattern shown in Fig. 2(c) is generated by segmenting the complete 834 μm by 834 μm in a 3×3 grid of 278 μm by 278 μm regions. It should be noted that with the described method it is possible that two apertures at the vertex between two diagonal regions can overlap. However, such occurrences are small enough compared to the full pattern size that this effect is negligible.

3. Fabrication

The device fabrication process is completed in two main stages. In the first stage, the metasurface grating design from Fig. 2(a) is fabricated on a quartz substrate. The diffraction efficiency is then measured on a custom-built setup. In the second stage, the RPD aperture pattern is etched through the Ag backplate, the SiO_2 substrate and the Ag tokens (but not through the quartz substrate). Finally, the diffraction efficiency of the final device is measured a second time. The fabrication procedure is described below.

A standard e-beam lithography (EBL) process was used to fabricate the metasurface grating. For adhesion purpose, a 3 nm layer of Cr was buried below each metal layer. The EBL was followed by a bi-layer resist lift-off technique due to the well-known advantages compared to single layer lift-off [32]. The fabricated metasurface pattern was imaged using scanning electron microscopy (SEM). As shown in Fig. 3(a) the fabricated nano tokens are well defined and match well with the simulated model. In the second stage, we used optical lithography to generate the RPD aperture pattern over the diffractive grating.

The final device front and back side imaged through an optical microscope are shown in Fig. 3(b) and (c), respectively. The dark square in (b) corresponds to the area where the grating structure was written on the front of the device. Due to the large scale of the image compared to the size of a single grating unit cell, the individual Ag tokens are not resolvable with the optical

Optical Materials EXPRESS

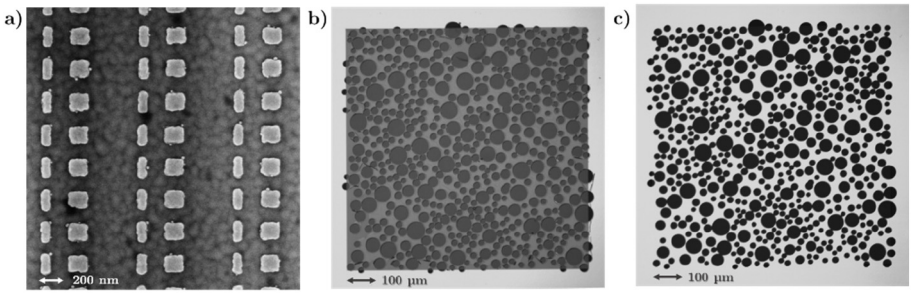

Fig. 3. Front and back of the metasurface device: (a) A SEM image of the nano-tokens forming the grating on the front of the device. The scale is 200 nm. (b) An optical microscope image of the front of the fabricated device. The dark square corresponds to the area patterned by the nano-tokens (shown in (a)) as seen through the optical microscope. The circles are the etched apertures that enable the see-though regime. The scale is 100 μm. (c) An optical microscope of the back of the device. Only the RPD aperture array is seen. The image is rotated in the same orientation as in (b) for easy comparison. The scale is 100 μm. The images have been converted to a black and white scale for better visualization.

microscope. A second device with a larger footprint (10 mm by 10 mm) was also fabricated with a similar RPD aperture pattern using the same fabrication method. The larger device is to be used to better understand the diffraction artifacts that get formed when light illuminates the back of the device where there are no nano-tokens (as further discussed in the next section).

4. Testing

The efficiency of the fabricated grating device was measured in the setup shown in Fig. 5(a). A Fianium WhiteLase micro supercontinuum laser was used combined with a 650 nm, 10 nm full-width-half-maximum (FWHM) bandpass filter as a light source. A linear polarizer was used to filter the desired TE polarization for which the grating was optimized. The sample was mounted on a custom-built stage. The stage provides all degrees of freedom required to align the sample and perform measurements for various angles of incidence. For this work the efficiency was measured for AOIs from 0 to 50 degrees. A collection arm was mounted on a rotation stage with the same center of rotation as the center of rotation of the sample that allowed capturing the light from various diffractive orders. Measurements in a region θ_{lim} around the Littrow angle were not possible as the collection arm occluded the input beam in that regime. A lens was used to collect the light from a desired order and to focus it on a Si photodiode connected to a pico-ammeter.

Given the Gaussian profile of the illumination beam provided by the laser, we overfilled the sample to better match the plane wave illumination used in the simulations. The total input power was measured before the sample using a second Si photodiode connected to the pico-ammeter. A knife edge experiment was used to measure the Gaussian beam profile which was then used to calculate the amount of light hitting the sample for each angle of incidence. The first diffractive order efficiency of the fabricated grating was first measured, and the final device efficiency was then measured again with a similar process once the RPD aperture pattern was added.

The larger (10 mm by 10 mm) sample was used to image the diffraction patterns formed when light passed through an RPD aperture array similar to diffraction effects formed when the main device was illuminated from the back. A white light LED with low coherence was used to illuminate the sample. Figure 4(g) shows the imaging setup used to take images of a negative 1951 USAF test target illuminated by the LED through a white diffusing paper. This setup represents well a scenario where a user (whose eye is modeled by the camera) looks at an object

Optical Materials EXPRESS

through an HWD with the RPD aperture array positioned on the combiner of the HWD. The see-through capabilities of the RPD aperture array can be properly evaluated in this configuration.

We also observed that the diffraction patterns formed by the RPD aperture arrays are most prominent when the sample is illuminated by a bright low coherence source like a flashlight or a ceiling lamp. If such devices are used in HWD combiners, the formed diffraction patterns as seen by the human eye could result in dangerous distractions. Examples of some real-life cases where that could be a problem are the user looking at streetlights or the lights from incoming cars. The setup in Fig. 5(c) was chosen to simulate these conditions with the camera representing the human eye, the sample representing the HWD combiner and the low coherence LED representing the bright illumination. Bandpass filters at 620 nm, 532 nm and 450 nm (10 nm FWHM for all three) were additionally used to simulate illumination at different visible wavelengths. The images were acquired using an Olympus PEN EPL-6 camera. It should be noted that the camera settings and the LED's brightness were chosen such that in Fig. 4 and 6 the camera has no saturated pixels while in Fig. 5 the camera sensor was saturated to model the human eye's retina saturating when looking at a bright source.

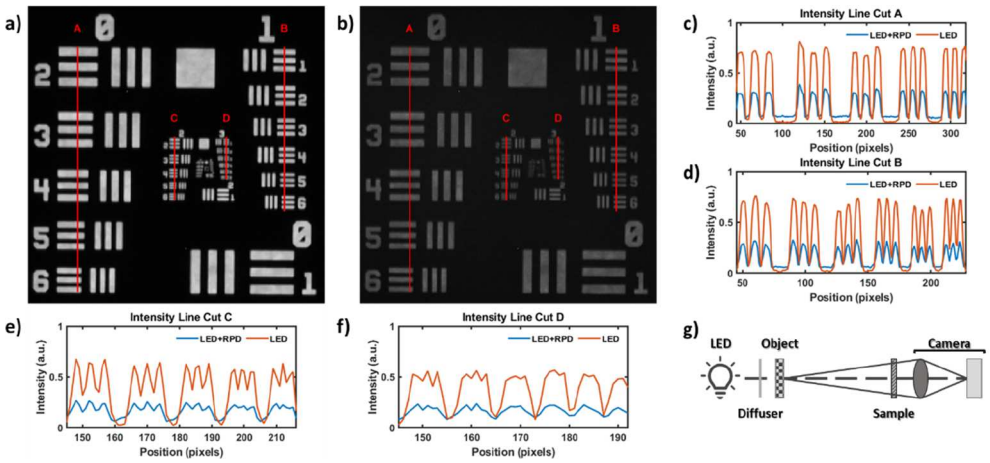

Fig. 4. (a) The intensity of an image of a negative 1951 USAF test target illuminated by a low coherence LED without the RPD pattern sample. (b) The intensity of an image of the target illuminated by the LED through the RPD pattern sample. (c-f) The intensity measured through line cuts A-D shown in (a) and (b). The intensity is measured in arbitrary units such that 1 corresponds to a fully saturated pixel on the camera detector and 0 corresponds to a fully dark pixel. (g) The imaging setup used to take the images of the test target.

Optical Materials EXPRESS

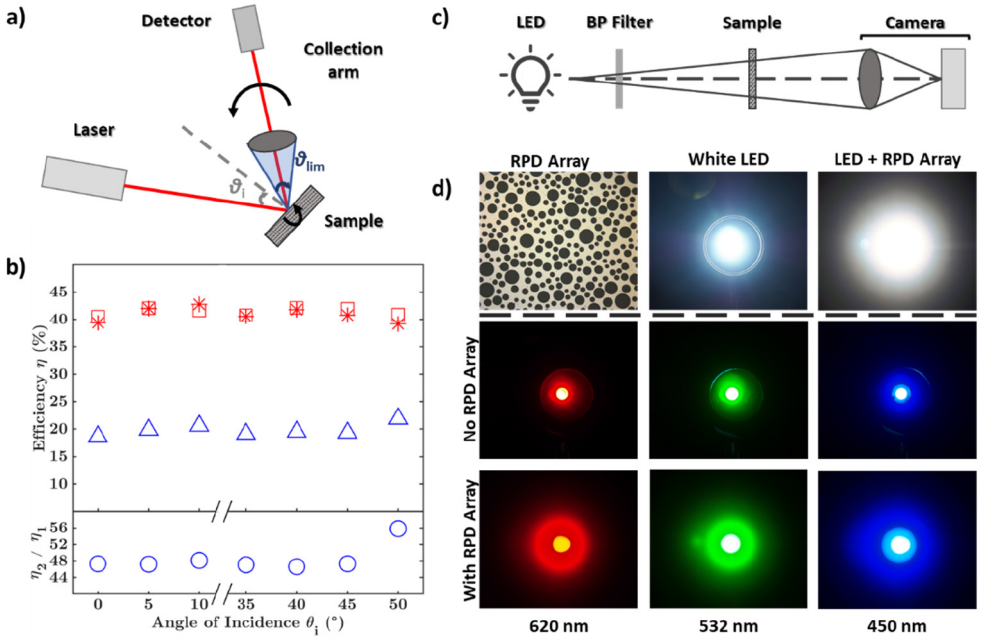

Fig. 5. (a) The experimental setup used to measure the diffraction efficiency; θ_{lim} is the angular region where the input and output arm collide and θ_{i} is the angle of incidence measured from the normal of the surface. (b) The experimental measurements of the device's efficiency before etching the apertures η_1 (red stars) and after etching the apertures η_2 (blue triangles). The red squares are the simulated values for the efficiency η_1. The blue circles show the ratio η_2/η_1 in percent. An x-axis break was used to emphasize the regions of interest where measurements were performed (the region left out corresponds to the regime where the input and output arm collide in the experimental setup). The uncertainty of the measurements is smaller than the size of the markers. (c) The experimental setup used to image the diffraction patterns formed by the 10 mm by 10 mm sample. (d) Imaging of the diffraction patterns formed by an RPD aperture array (top left corner) on the 10 mm by 10 mm sample. The pixels in the center of the images are saturated on the camera's detector.

Optical Materials EXPRESS

5. Results and discussion

Figure 4 demonstrates the see-through functionality of the RPD aperture array using the 10 mm by 10 mm sample (an optical microscope image of the used sample is shown in the top left corner of Fig. 5(d)). As it can be seen from the line cut intensity plots shown in Fig. 4. (c-f) on average the intensity of the image when seen through the RPD aperture array is about 40-50% lower than the intensity of the image seen without the sample. This matches well with the 50% target transmission ratio for the fabricated RPD aperture array. In Fig. 4(c), additional contrast loss in the image with the RPD pattern is observed (blue curve) due to the black regions between the neighboring groups of three white stripes having higher intensity than 0 (while the orange curve reaches close to 0 in those regions). This is due to the diffraction effects from the aperture array. On average that "leaked" light intensity is about 10-15% from the peak intensity of the image without the RPD pattern and is observed also in Fig. 4(d) and (e).

As we move from Fig. 4(c) to Fig. 4(f) the line cuts A-D, whose intensity is plotted, represent regions of the test target with higher spatial resolution, increasing from 1.12 line pairs/mm at the top of line cut A to 14.25 line pairs/mm at the bottom of line cut D. Naturally, due to the limited performance of the used camera, the contrast (ratio between the peaks and lows of the intensity curves) decreases for the higher spatial frequencies and the peaks corresponding to each white stripe become less distinguishable. However, most of the peaks that are distinguishable in the image without the RPD pattern are also distinguishable in the image with the RPD pattern. Thus, despite of the lower overall contrast due to the 50% see-through ratio and the additional diffraction artifacts the RPD pattern still provides comparable see-through experience. It should be noted that in Fig. 4(f) the spatial resolution of the white strips is high enough that it is impossible to resolve two neighboring strips for both the image with and without the RPD aperture array, showing that the loss in resolution is mostly due to the performance of the camera and not the RPD sample. The black regions between neighboring groups of three stripes have the same intensity for both the blue and orange curve which confirms that the blur caused by the camera performance is the limiting factor in this region of low resolution and not the diffraction effects from the RPD aperture array.

Figure 5(b) presents the efficiency results for the fabricated grating device in reflection. First, it can be seen that the experimentally measured first order efficiency η_1 (red stars) of the diffractive grating was in good agreement with the simulated values (red squares). The efficiency η_2 of the final device including the diffraction grating and the RPD aperture pattern is also shown (blue triangles) as well as the ratio η_2/η_1 (bottom inset).

The see-through ratio for the fabricated device was chosen to be 50%. As previously discussed, this setting means that 50% of the light illuminating the back of the device will be transmitted through. It also means that 50% of the light hitting the front of the sample will not interact with the nano-tokens forming the grating (as they were etched away at the location of the RPD apertures) and hence will not contribute to the diffracted light. The result is an efficiency η_2 that theoretically should be half of the initial efficiency η_1 of the grating before the RPD aperture array was etched. It should be noted that the source used in the experiments was not an ideal plane wave but a Gaussian that could cause deviations from the desired transmission ratio (and the corresponding η_2/η_1 ratio). However, as previously stated the incoming beam overfills the sample. Furthermore, the diameters of the RPD apertures (<30 μm) are significantly smaller than the $1/e^2$ beam diameter of the Gaussian beam (~2.2 mm) and hence, the beam intensity over each RPD aperture is relatively constant. We further verified this assumption by numerically calculating the light transmitted by each individual aperture and showed that for the used Gaussian beam the expected η_2/η_1 ratio varies by less than 0.25% from the desired 50% target for all AOIs of interest. The average (averaged over all AOIs from 0 to 50 degrees) experimentally measured ratio η_2/η_1 is 51.33% with a standard deviation of 5.28 as seen in the inset of Fig. 5(b).

Optical Materials EXPRESS

To study the effects of the RPD pattern under bright light low coherence elimination we also used the larger 10 mm by 10 mm sample. The images in Fig. 5(d) (besides the optical microscope image of the sample in the top left inset) were taken with the setup shown in Fig. 5(c) and described in detail in the previous section. All images were taken with the camera sensor saturated at the center of the image to properly simulate the similar saturation effect, looking at a bright light would have on a user's retina. An image of the white LED source without a bandpass filter and without the RPD aperture array pattern is shown in top row, middle inset. The image of the diffracted white light through the RPD aperture array with no bandpass filter is shown in the top right corner. The middle row shows images of the LED source without the RPD aperture array through bandpass filters of 620 nm, 532 nm and 450 nm, from left to right correspondingly. The bottom row shows the light diffracted through the RPD aperture array for each of the corresponding wavelengths. As can be seen by the bottom row and the top, right figure, the diffracted light forms a halo around the original source but no sharp features or structures like streaks, speckle or rings are observed. The only exception is a single dark ring for the blue light which is however not present for the other wavelengths or for the white diffracted light. This behavior is a significant improvement to alternative methods where the apertures are not distributed randomly or have the same diameter.

To better quantify the magnitude of the diffraction halo we took two more images of the white LED with and without the RPD aperture array without the camera saturating as shown in Fig. 6(a) and (b). The intensity through the line cuts shown in (a) and (b) is shown in Fig. 6(c). An overall decrease in intensity is observed as expected due to the semi-transparent properties of the RPD pattern. The diffraction halo caused by the aperture array is evident by the wings of the blue curve surrounding the area of high intensity at the center of the LED. The peak of those wings is about 10% of the peak intensity without the RPD pattern which is comparable to the diffraction effects seen in Fig. 4.

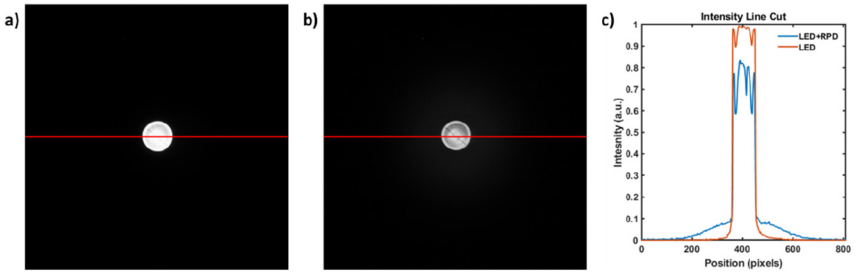

Fig. 6. (a) The intensity of an image of the LED taken in the setup shown in Fig. 5(c) without the RPD pattern sample. (b) The intensity of an image of the LED as seen through the RPD pattern sample. (c) The intensity through the line cuts shown in (a) and (b). The intensity is measured in the same arbitrary units used in Fig. 4.

6. Conclusion

In this paper, we proposed and reported on an alternative approach to an ultrathin 2-6 nm Ag backplate to achieve semi-transparency while preserving the anomalous reflection. The approach consists in etching a set of circular apertures with diameters much larger than the wavelength of operation. With this approach, we have demonstrated the design, fabrication and performance of a dual function metasurface based device that can be used in reflection as a grating while also transmitting light when illuminated from the back without introducing undesirable diffraction artifacts. The metasurface grating has 1200 lp/mm grating spacing and is optimized to have a ~20% efficiency in the first diffractive order at 650 nm illumination. An RPD aperture array was

Optical Materials EXPRESS

used to provide the desired transmission ratio of 50%. The light diffracted through this array does not form any sharp features or structures like streaks and rings making it viable for use as part of a visual system. The see-through performance of the RPD pattern was demonstrated. At high resolution imaging, diffraction blur was observed with intensity of 10-15% of the peak intensity without the aperture array. At low resolution imaging, the blur from the imaging optics was predominant and was not noticeably increased by diffraction effects from the see-through RPD pattern. The dual functionality of this see-through metasurface diffraction grating can be useful in a variety of consumer optical systems including waveguide or combiner based HWDs.

Funding

Center for Emerging and Innovative Sciences (100012430); Link Foundation (100005238).

Acknowledgments

We thank Gustavo Gandara-Montano for stimulating technical discussions.

References

1. O. Cakmakci and J. P. Rolland, "Examples of HWD Architectures: Low-, mid- and wide-field of fiew designs," in *Handbook of Visual Display Technology*, J. Chen, W. Cranton, and M. Fihn, eds. (Springer, 2012).
2. B. Kress and T. Starner, "A review of head-mounted displays (HMD) technologies and applications for consumer electronics," in *Proc. SPIE 8720, Photonic Applications for Aerospace, Commercial, and Harsh Environments IV*, (2013).
3. M. J. Hayford and O. Cakmakci, "Optical components for head-worn displays," in *Handbook of Visual Display Technology*, J. Chen, W. Cranton, and M. Fihn, eds. (Springer, 2016).
4. Z. Liu, Y. Pang, C. Pan, and Z. Huang, "Design of a uniform-illumination binocular waveguide display with diffraction gratings and freeform optics," Opt. Express **25**(24), 30720–30731 (2017).
5. A. Travis, "Wide field-of-view virtual image projector," U.S. patent application 20,130,021,392 A1 (January 24, 2013).
6. A. Travis, "Wide field-of-view virtual image projector," U.S. patent application 20,130,329,301 A1 (December 12, 2013).
7. T. Levola, "Diffractive optics for virtual reality display," J. Soc. Inf. Disp. **14**(5), 467–475 (2006).
8. H. Mukawa, K. Akutsu, I. Matsumura, S. Nakano, T. Yoshida, M. Kuwahara, and K. Aiki, "A full-color eyewear display using planar waveguides with reflection volume holograms," J. Soc. Inf. Disp. **17**(3), 185–193 (2009).
9. H. Mukawa, K. Akutsu, I. Matsumura, S. Nakano, T. Yoshida, M. Kuwahara, K. Aiki, and M. Ogawa, "A full color eyewear display using holographic planar waveguides," Dig. Tech. Pap. - Soc. Inf. Disp. Int. Symp. **39**(1), 89–92 (2008).
10. A. Bauer and J. P. Rolland, "Visual space assessment of two all-reflective, freeform, optical see-through headworn displays," Opt. Express **22**(11), 13155–13163 (2014).
11. J. P. Rolland, A. N. Vamivakas, A. Bauer, D. K. Nikolov, and F. Cheng, "Augmented reality display," U.S. Provisional Pat. Ser. No. 62/679,505, filed 06/01/2018.
12. X. Chen, L. Huang, H. Mühlenbernd, G. Li, B. Bai, Q. Tan, G. Jin, C.-W. Qiu, S. Zhang, and T. Zentgraf, "Dual-polarity plasmonic metalens for visible light," Nat. Commun. **3**(1), 1198 (2012).
13. A. Pors and S. I. Bozhevolnyi, "Efficient and broadband quarter-wave plates by gap-plasmon resonators," Opt. Express **21**(3), 2942–2952 (2013).
14. A. Pors, M. G. Nielsen, and S. I. Bozhevolnyi, "Broadband plasmonic half-wave plates in reflection," Opt. Lett. **38**(4), 513–515 (2013).
15. F. Cheng, L. Ding, L. Qiu, D. Nikolov, A. Bauer, J. P. Rolland, and A. N. Vamivakas, "Polarization-switchable holograms based on efficient, broadband multifunctional metasurfaces in the visible regime," Opt. Express **26**(23), 30678–30688 (2018).
16. S. Sun, K. Y. Yang, C. M. Wang, T. K. Juan, W. T. Chen, C. Y. Liao, Q. He, S. Xiao, W.-T. Kung, G.-Y. Guo, L. Zhou, and D. P. Tsai, "High-efficiency broadband anomalous reflection by gradient meta-surfaces," Nano Lett. **12**(12), 6223–6229 (2012).
17. A. Pors and S. I. Bozhevolnyi, "Plasmonic metasurfaces for efficient phase control in reflection," Opt. Express **21**(22), 27438–27451 (2013).
18. Z. Li, E. Palacios, S. Butun, and K. Aydin, "Visible-frequency metasurfaces for broadband anomalous reflection and high-efficiency spectrum splitting," Nano Lett. **15**(3), 1615–1621 (2015).
19. A. L. Kitt, J. P. Rolland, and A. N. Vamivakas, "Visible metasurfaces and ruled diffraction gratings: a comparison," Opt. Mater. Express **5**(12), 2895–2901 (2015).

Optical Materials EXPRESS

20. T. Coan, G. S. Barroso, R. A. F. Machado, F. S. de Souza, A. Spinelli, and G. Motz, "A novel organic-inorganic PMMA/polysilazane hybrid polymer for corrosion protection," Prog. Org. Coat. **89**, 220–230 (2015).
21. T. Coan, G. S. Barroso, G. Motz, A. Bolzán, and R. A. F. Machado, "Preparation of PMMA/hBN composite coatings for metal surface protection," Mater. Res. **16**(6), 1366–1372 (2013).
22. F. Cheng, J. Gao, T. S. Luk, and X. D. Yang, "Structural color printing based on plasmonic metasurfaces of perfect light absorption," Sci. Rep. **5**(1), 11045 (2015).
23. F. Cheng, X. D. Yang, D. Rosenmann, L. Stan, D. Czaplewski, and J. Gao, "Enhanced structural color generation in aluminum metamaterials coated with a thin polymer layer," Opt. Express **23**(19), 25329–25339 (2015).
24. D. K. Nikolov, F. Cheng, N. Basaran, A. Bauer, J. P. Rolland, and A. N. Vamivakas, "Long-term efficiency preservation for gradient phase metasurface diffraction gratings in the visible," Opt. Mater. Express **8**(8), 2125–2130 (2018).
25. A. Axelevitch, B. Gorenstein, and G. Golan, "Investigation of Optical Transmission in Thin Metal Films," Phys. Procedia **32**, 1–13 (2012).
26. S. Link, C. Burda, Z. L. Wang, and M. A. El-Sayed, "Electron dynamics in gold and gold–silver alloy nanoparticles: the influence of a nonequilibrium electron distribution and the size dependence of the electron–phonon relaxation," J. Chem. Phys. **111**(3), 1255–1264 (1999).
27. M. Fox, "Molecular Materials," in *Optical Properties of Solids* (Oxford University Press, 2010).
28. P. D. Lee, C. T. LaBree, and R. A. Freibrun, "Fresnel diffraction patterns of an array of circular apertures," J. Opt. Soc. Am. **57**(9), 1115–1120 (1967).
29. R. Bergsten and S. Huberty, "White-light Fresnel diffraction by a circular aperture," J. Opt. Soc. Am. **67**(5), 643–647 (1977).
30. D. S. Burch, "Fresnel diffraction by a circular aperture," Am. J. Phys. **53**(3), 255–260 (1985).
31. Inc. Lumerical Solutions.
32. T. Deyu, L. Ming, S. Liwei, X. Changqing, and Z. Xiaoli, "A ZEP520-LOR bilayer resist lift-off process by e-beam lithography for nanometer pattern transfer," in *7th IEEE Conference on Nanotechnology* (2007).